ELSEVIER

Chemical Engineering Journal 84 (2001) 503–516

Chemical Engineering Journal

www.elsevier.com/locate/cej

Classification of static and dynamic behavior in a fluidized-bed catalytic reactor

Abdelhamid Ajbar [a,*], Khalid Alhumazi [a], S.S.E.H. Elnashaie [b]

[a] *Department of Chemical Engineering, King Saud University, P.O. Box 800, Riyadh 11421, Saudi Arabia*
[b] *Department of Chemical Engineering, Auburn University, Auburn, AL, USA*

Received 27 November 1999; received in revised form 8 November 2000; accepted 8 November 2000

Abstract

The singularity theory and continuation techniques are combined to classify the static and dynamic behavior of a non-isothermal gas–solid fluidized-bed catalytic reactor with consecutive exothermic reactions $A \xrightarrow{k_1} B \xrightarrow{k_2} C$. It is shown that the double limit variety with five solutions is the highest static singularity the model can predict. The model is also capable of predicting self sustained oscillations for a wide range of Lewis numbers. The effect of the model parameters on its static and dynamic bifurcation is analyzed. Practical criteria are also derived for the effect of the branching phenomena on the yield of the intermediate product in the reactions network.

Keywords: Static; Dynamic; Catalytic reactor

1. Introduction

Non-linear models of reactive systems can exhibit a variety of behavior depending on the values of the system parameters. For certain values of the parameters the reactive system can exhibit simple or complex quasi-periodic as well as chaotic oscillations. An important objective for the analysis of dynamics of reactive systems is the classification of the parameter space into regions where different types of behavior can be delineated. Besides increasing the understanding of the reactive system, this classification can have practical impact on the operation of the reactor, since it can allow the determination of boundaries between safe and runaway regions and the delineation of regions of undesired oscillations or unstability. The classification of the parameter space is however a challenging task since the number of parameters in any reactive system model can be quite large. A systematic classification in the multidimensional parameter space can be a difficult task without appropriate theoretical means. Various nonlinear dynamics tools have been used in the literature for the analysis of reactive systems. Among them the singularity theory [1] is recognized as being a useful tool since it can provide a general framework for classifying branching phenomena in which different kinds of multiplicity in the nonlinear model can be expected. The theory has found several applications in the chemical engineering field since Balakotaiah and Luss [2] analyzed the multiplicity phenomenon of the simple CSTR. D'anna et al. [3] and Alhumazi and Aris [4] provided other applications of the theory in their study of the stability characteristics of autocatalytic reactive systems. Most of the comprehensive studies in the literature focused on homogenous and pseudo-homogenous reactive systems. Recently Subramanian and Balakotaiah [5] extended the classification to a heterogeneous well-mixed reactor.

In this contribution we extend the study of heterogeneous systems by a classification of the static and dynamic behavior of a non-isothermal gas–solid catalytic bubbling fluidized-bed reactor. A consecutive reaction network $A \xrightarrow{k_1} B \xrightarrow{k_2} C$ is taking place in the reactor where the desired product is the intermediate component (B). The problem has practical applications. Besides the important industrial uses of fluidized-bed technology, there are cases in petrochemical industry where the reactor is operated in a multiplicity region or where the maximum yield of the intermediate product occurs at an unstable point. These situations include the industrially important FCC unit [6], the partial oxidation of *o*-xylene [7] as well as oxidative dehydrogenation reactions such as the oxidative

Abbreviations: HB, Hopf bifurcation point; SLP, static limit point

*Corresponding author. Fax: +966-1-467-8770.
E-mail address: aajbar@ksu.edu.sa (A. Ajbar).

1385-8947/01/$ – see front matter
PII: S1385-8947(00)00373-9

Nomenclature

a	two-phase parameter ($=Q_E H A_C/G_C$)
A	cross-sectional area of the bed (cm^2)
A_C	cross-sectional area of the bed occupied by bubble phase (cm^2)
A_I	cross-sectional area of the bed occupied by dense phase (cm^2)
C_i	concentration of component i in the dense phase ($kg\,mol\,cm^{-3}$)
C_{if}	feed concentration of component i ($kg\,mol\,cm^{-3}$)
$\bar{C}_i$	concentration of the component i in the bubble phase ($kg\,mol\,cm^{-3}$)
$\bar{C}_m$	total concentration of active sites (kg mol/kg catalyst)
C_{pf}	specific heat of gas ($kJ\,kg^{-1}\,K$)
C_{ps}	specific heat of the catalyst ($kJ\,kg^{-1}\,K$)
C_{ref}	reference concentration ($kg\,mol\,cm^{-3}$)
E_1	activation energy for the reaction A → B ($kJ\,kg\,mol^{-1}$)
E_2	activation energy for the reaction B → C ($kJ\,kg\,mol^{-1}$)
G_C	volumetric gas flow rate in bubble phase ($m^3\,s^{-1}$)
G_I	volumetric gas flow rate in dense phase ($m^3\,s^{-1}$)
H	expanded bed height for the fluidized-bed (cm)
$-\Delta H_1$	overall heat of A → B ($kJ\,kg\,mol^{-1}$)
$-\Delta H_2$	overall heat of B → C ($kJ\,kg\,mol^{-1}$)
k_1	surface reaction rate constant for A → B (s^{-1})
k_1'	pre-exponential factor for $\bar{k}_1$ ($cm^3\,kg^{-1}$ catalyst s)
$\bar{k}_1$	reaction rate constant for A → B ($=k_1 K_A \bar{C}_m$) ($cm^3\,kg^{-1}$ catalyst s)
k_2	surface reaction rate constant for B → C (s^{-1})
k_2'	pre-exponential factor for $\bar{k}_2$
$\bar{k}_2$	reaction rate constant for B → C ($=k_2 K_B \bar{C}_m$) ($cm^3\,kg^{-1}$ catalyst s)
K_A	adsorption equilibrium constant for component A ($cm^3\,kg\,mol^{-1}$)
K_B	adsorption equilibrium constant for component B ($cm^3\,kg\,mol^{-1}$)
Le_i	Lewis number of component i (heat capacity/mass capacity of component i)
Q_E	assumed in the model to be equal to Q_{Ei} and Q_H (s^{-1})
Q_{Ei}	mass exchange coefficient (s^{-1})
Q_H	heat exchange coefficient (s^{-1})
r_i	rate of reaction of component i ($kg\,mol\,kg^{-1}$ catalyst s)
R_i	rate of disappearance of component i ($kg\,mol\,kg^{-1}$ catalyst s)
t	normalized time (time/heat capacity of the system)
T	temperature of the dense phase (K)
$\bar{T}$	temperature of the bubble phase (K)
$\bar{T}_f$	feed temperature (K)
T_{ref}	reference temperature (K)
U	superficial flow velocity of the gas in the bed ($cm\,s^{-1}$)
U_{mf}	minimum fluidization velocity of the solid ($cm\,s^{-1}$)
X_A	dimensionless dense phase concentration of the reactant A
X_B	dimensionless dense phase concentration of the product B
X_{if}	dimensionless feed concentration of component i
$\bar{X}_{BH}$	dimensionless bubble phase concentration of B at the exit of the reactor
Y	dimensionless dense phase temperature
Y_f	dimensionless feed temperature to the reactor (base value)

Greek symbols

α_1	dimensionless pre-exponential factor for A → B ($=(1-\epsilon)\rho_s k_1'$) (s^{-1})
α_2	dimensionless pre-exponential factor for B → C ($=(1-\epsilon)\rho_s k_2'$) (s^{-1})
β_1	dimensionless overall exothermicity factor for A → B ($=-(\Delta H)_1 C_{ref}/\rho_f C_{pf} T_{ref}$)
β_2	dimensionless overall exothermicity factor for B → C ($=-(\Delta H)_2 C_{ref}/\rho_f C_{pf} T_{ref}$)
$\bar{\beta}$	reciprocal of the residence time of the bed
ϵ	voidage occupied by the gas in the dense phase
ϕ_H	dimensionless effective heat capacity of the dense phase ($=(1-\epsilon)C_{ps}\rho_s/C_{pf}\rho_f$)
ϕ_i	dimensionless effective mass capacity of the component i ($=\epsilon+(1-\epsilon)\rho_s K_i \bar{C}_m$)
γ_1	dimensionless activation energy for A → B ($=E_1/RT_{ref}$)
γ_2	dimensionless activation energy for B → C ($=E_2/RT_{ref}$)
ρ_s	density of the solid catalyst ($kg\,catalyst\,cm^{-3}$)
ρ_f	density of the gas ($kg\,cm^{-3}$)

dehydrogenation of butene to butadiene [8] and ethylbenzene to styrene [9].

The objectives of this work are two-fold. The first objective is to provide a unified framework, using the singularity theory and continuation techniques for the analysis of static bifurcation induced in the reactor by the consecutive reactions network. The relative simplicity of the model equations allows the description of the steady-state

behavior of the reactor in form of a single algebraic equation. It is shown that a general and practical picture of the different stability phenomena in the reactor can be drawn in a systematic and quite useful manner. The practical effect of these branching phenomena on the yield of the intermediate product are also discussed. The second objective of the paper is to study the dynamic bifurcation of the reactor. In contrast to linear systems, it is known that structurally stable periodic solutions can exist for nonlinear systems. The ability of the reactor model to predict sustained oscillations is investigated. A strong focus is made on the effect of Lewis numbers on the existence and the nature of oscillatory behavior in the reactor. It is known that for gas–solid catalytic systems, the mass capacities of a strongly chemisorbed component may exceed the heat capacity of the system and the Lewis numbers may vary form unity [10]. The important effect of chemisorption capacities on the dynamic behavior of gas–solid catalytic systems has been recognized by a number of investigators [11–13]. The combination of both static and dynamic branching phenomena helps to construct a complete picture of the different modes of behavior in the reactor.

The organization of the paper includes a presentation of the model of the reactor. Static analysis is carried out first followed by a study of the dynamic behavior. For the sake of clarity, the mathematical details of the singularity theory are omitted from the analysis. Most of the related materials about the theory can be found in the referenced textbook [1] or in the useful summaries provided by Alhumaizi and Aris [4].

2. Process model

The equations in dimensionless form for the reactor dense phase material and energy balances are given by the following three non-linear differential equations:

$$\frac{1}{Le_{\mathrm{A}}}\frac{\mathrm{d}X_{\mathrm{A}}}{\mathrm{d}t} = \bar{\beta}(X_{\mathrm{A_f}} - X_{\mathrm{A}}) - \alpha_1 \exp\left(-\frac{\gamma_1}{Y}\right) X_{\mathrm{A}} \tag{1}$$

$$\frac{1}{Le_{\mathrm{B}}}\frac{\mathrm{d}X_{\mathrm{B}}}{\mathrm{d}t} = \bar{\beta}(X_{\mathrm{B_f}} - X_{\mathrm{B}}) + \alpha_1 \exp\left(-\frac{\gamma_1}{Y}\right) X_{\mathrm{A}} - \alpha_2 \exp\left(-\frac{\gamma_2}{Y}\right) X_{\mathrm{B}} \tag{2}$$

$$\frac{\mathrm{d}Y}{\mathrm{d}t} = \bar{\beta}(\bar{Y}_{\mathrm{f}} - Y) + \alpha_1\beta_1 \exp\left(-\frac{\gamma_1}{Y}\right) X_{\mathrm{A}} + \alpha_2\beta_2 \exp\left(-\frac{\gamma_2}{Y}\right) X_{\mathrm{B}} \tag{3}$$

where X_{A}, X_{B} are the dimensionless concentrations of components A and B in the reactor dense phase, and Y is the dimensionless dense phase temperature. A schematic diagram of the two-phase model of the reactor is given in Fig 1. The bubble-phase mass and heat balances equations

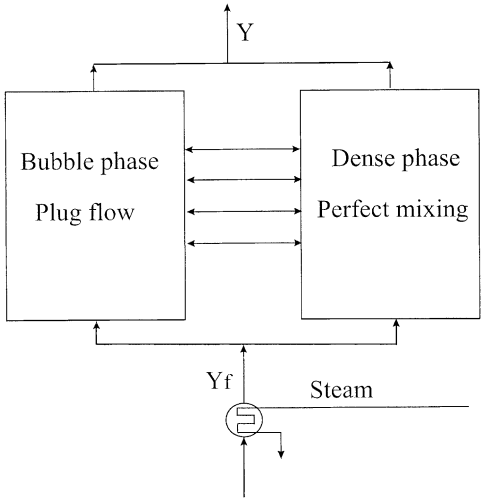

Fig. 1. Schematic diagram of the two-phase model of the reactor.

are assumed to be at pseudo-steady state because of negligible mass and heat capacities. The Le_i are the Lewis numbers representing the ratio between the heat capacity of the system and the mass capacities for the components. The $\alpha_i = (1-\epsilon)\rho_{\mathrm{s}}k_i$ are the normalized pre-exponential factors for the two reactions while the $\beta_i = -\Delta H_i/\rho_{\mathrm{f}}C_{p\mathrm{f}}T_{\mathrm{f}}$ represent the dimensionless overall exothermicity factors. The γ_i are the dimensionless activation energies and $\bar{\beta}$ is the reciprocal of the effective residence time of the bed.

The model assumptions and detailed derivation are summarized in Appendix A. This two-phase model represents one of the relatively few dynamic models in the literature for non-isothermal fluidized-bed catalytic reactors that take into its formulation the heats and mass transfer resistances between the dense and bubble phase. The two-phase models were used by Choi and Ray [14] to model and control industrial polyethylene reactors. They were also used for the dynamic analysis of type IV industrial fluid catalytic cracking units [15].

Before we present the results of the analysis a final note should be made about the effect of Lewis numbers Le_{A} and Le_{B}. Dynamic models that assume negligible chemisorption capacities of the different component on the catalyst yield large values for Le_{A} and Le_{B}. The mass balance equations (1)–(3), therefore, predict extremely fast response for concentrations X_{A} and X_{B} compared with the response of the temperature Y. In this case X_{A} and X_{B} can be assumed at pseudo-steady state all the time. Under these physically questionable assumptions the system becomes dynamically one-dimensional and most of the dynamic characteristic of the system are therefore lost. In the present model the chemisorption capacity of the solid catalyst in the dense phase is taken into consideration and the richness of the dynamics associated with the relaxation of these assumptions are demonstrated.

3. Static bifurcation

The steady-state equations are obtained by setting the left-hand sides of Eqs. (1)–(3) to zero. Eqs. (1) and (2) in particular would yield

$$X_{\mathrm{A}} = \frac{\bar{\beta} X_{\mathrm{A_f}}}{\bar{\beta} + \alpha_1 \exp(-\gamma_1/Y)} \tag{4}$$

and

$$X_{\mathrm{B}} = \frac{\bar{\beta} X_{\mathrm{B_f}} + \alpha_1 X_{\mathrm{A}} \exp(-\gamma_1/Y)}{\bar{\beta} + \alpha_2 \exp(-\gamma_2/Y)} \tag{5}$$

By introducing Eq. (4) into Eq. (5) and then into the steady-state form of Eq. (3), a single algebraic equation is obtained for Y,

$$\begin{aligned} F(Y) :=\ & \alpha_1\alpha_2\bar{\beta} \exp\left(-\frac{\gamma_1+\gamma_2}{Y}\right) f_1(Y) \\ & + \alpha_1\bar{\beta}^2 \exp\left(-\frac{\gamma_1}{Y}\right) f_2(Y) \\ & + \alpha_2\bar{\beta}^2 \exp\left(-\frac{\gamma_2}{Y}\right) f_3(Y) - \bar{\beta}^3(Y - Y_{\mathrm{f}}) \end{aligned} \tag{6}$$

with

$$f_1(Y) := (\beta_1 + \beta_2) X_{\mathrm{A_f}} + \beta_2 X_{\mathrm{B_f}} - Y + Y_{\mathrm{f}} \tag{7}$$

$$f_2(Y) := \beta_1 X_{\mathrm{A_f}} - Y + Y_{\mathrm{f}} \tag{8}$$

$$f_3(Y) := \beta_2 X_{\mathrm{B_f}} - Y + Y_{\mathrm{f}} \tag{9}$$

The steady-state equation (Eq. (6)) depends on all the model parameters expect the Lewis numbers Le_{A} and Le_{B}.

We are interested in the way the steady state Y depends on the positive system parameters. The feed temperature Y_{f} appearing explicitly in Eq. (6) is selected to be the bifurcation parameter. For this kind of equation the singularity theory defines two types of codimension-one singularities that can be found, namely hysteresis (Fig. 2(a)), isola–mushroom (Fig. 2(b) and (c)) and double limit (Fig. 2(d) and (e)). Pitchfork (codimension-two) (Fig. 2(f)) singularity can also be defined for the algebraic equation.

3.1. Hysteresis singularity

The conditions for the appearance/disappearance of a hysteresis loop are

$$F = F_Y = F_{YY} = 0 \tag{10}$$

that is the point should be a steady-state point ($F = 0$) and the first two partial derivative of F with respect to Y must vanish. In addition a number of other derivatives must remain non-zero, namely $F_{Y_{\mathrm{f}}}$, $F_{YY_{\mathrm{f}}}$ and F_{YYY}.

The above conditions form the boundaries of the hysteresis singularity. Fig. 3 shows these boundaries in the parameter space $(X_{\mathrm{A_f}}, \bar{\beta})$. The values of the other parameters are shown in Table 1. The boundaries divide the parameter space in four regions. The conditions $F_{Y_{\mathrm{f}}}$, $F_{YY_{\mathrm{f}}}$ and F_{YYY} were evaluated numerically along the hysteresis surface and no point was found to violate the conditions. When crossing the boundaries in Fig. 3, the number of static limit points (SLP) in the bifurcation diagrams increases/decreases by two. Region (a) is characterized, for any combinations of $X_{\mathrm{A_f}}$ and $\bar{\beta}$ by the absence of static limit points, i.e. unique steady-state solution. The expected behavior in this region is shown in the continuity diagram of Fig. 4(a_1) obtained, for example with $(X_{\mathrm{A_f}}, \bar{\beta}) = (0.15, 0.2)$. The software package AUTO [16] was used to generate the continuity diagrams. A monotonic increase in the temperature Y with the feed temperate Y_{f} can be observed. The yield of the desired intermediate product, shown in Fig. 4(a_2), reaches its maximum of 0.91841 at the feed temperature of 0.81367. When crossing the boundary separating regions (a) and (b) in Fig. 3 two static limit points are born. A hysteresis with a maximum three steady-state solutions characterize the nature of the system in region (b). Fig. 5(b_1) shows an example of the behavior in this region obtained with $(X_{\mathrm{A_f}}, \bar{\beta}) = (0.4, 0.2)$. The maximum yield 0.91126 occurs (Fig. 5(b_2)) at the stable branch at the value of $Y_{\mathrm{f}} = 0.89265$. Region (c) on the other hand is characterized by the presence of four limit points since two extra SLP are born when crossing the boundary separating regions (b) and (c). A maximum of five steady-state solutions are expected in this region, as it can be seen in the continuity diagram of Fig. 6(c_1) obtained with $(X_{\mathrm{A_f}}, \bar{\beta}) = (0.6, 0.2)$. In addition to two stable low and high temperature branches a third stable branch exists in the middle. The maximum yield of 0.91124 occurs at the stable branch at $Y_{\mathrm{f}} = 0.81367$ (Fig. 6(c_2)). When crossing the region (c) two limit points disappear and the system is characterized

Table 1
Model nominal parameters used in simulations

Parameter	Value
A	3000 cm^2
U	10.0 cm s^{-1}
U_{mf}	0.875 cm s^{-1}
ϕ	1.8
α	19.5
ϵ	0.4
Q_{E}	2.0
H	100 cm
α_1	10^8 s^{-1}
α_2	10^{11} s^{-1}
β_1	0.4
β_2	0.6
γ_1	18.0
γ_2	32.0
Le_{A}	1.0
Le_{B}	0.454545
$X_{\mathrm{A_f}}$	1.0
$X_{\mathrm{B_f}}$	0.0
Y_{f}	0.5
$\bar{\beta}$	0.2

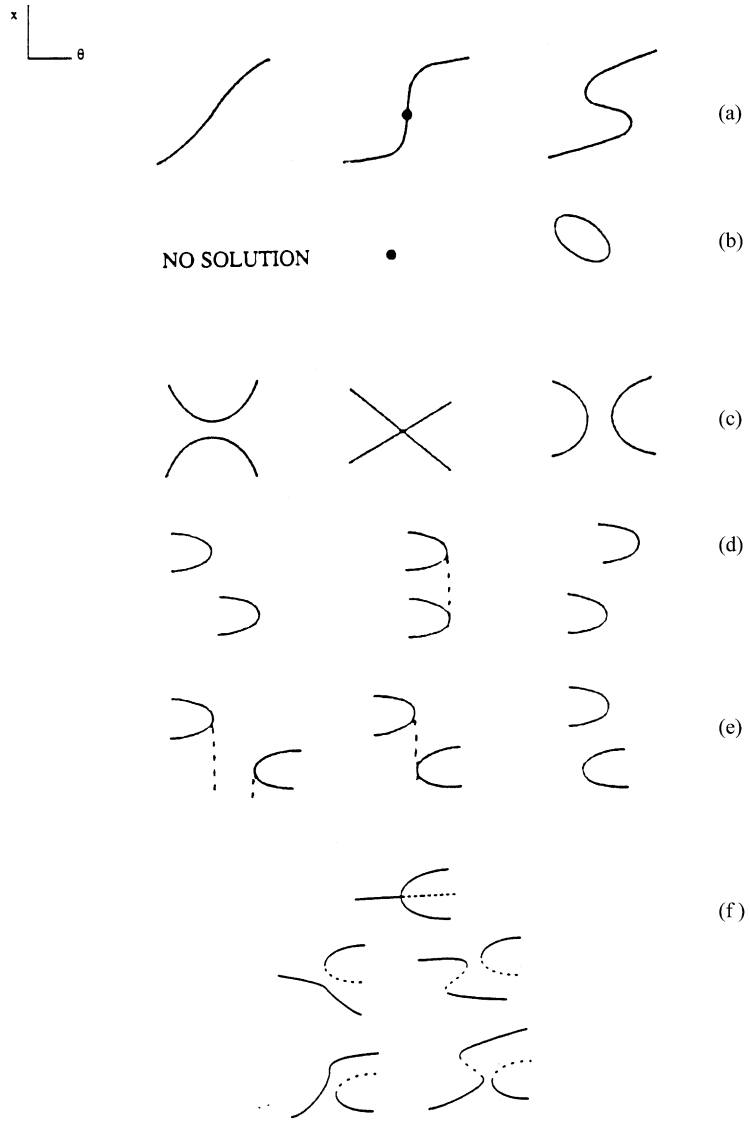

Fig. 2. Examples of singularities: (a) hysteresis; (b) isola; (c) mushroom; (d–e) double limit; (f) pitchfork.

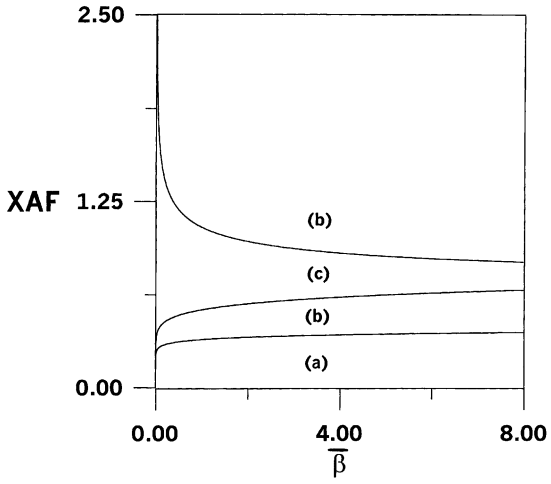

Fig. 3. Branch sets for the hysteresis singularity in the parameter space $(X_{A_f}, \bar{\beta})$.

as in region (b) with the existence of three steady solutions for some range of the feed temperature. In all these cases, hysteresis introduces dangerous operations for the reactor since any abrupt change in the operating parameters can cause the system to jump from high yield points to low yield operating points.

The same three modes of behavior can be found in the parameter space (X_{A_f}, γ_1) and (X_{A_f}, γ_2) (Fig. 7(a) and (b)). It can be seen from these figures that for given values of dimensionless activation energies γ_1 and γ_2, the multiplicity region is favored by high values of the feed concentration X_{A_f}. Moreover, smaller values of γ_1 and higher values of γ_2 also favor the occurrence of multiplicity. Fig. 8 shows an example of behavior for region (b) of Fig. 7(a) for values of $(X_{A_f}, \bar{\beta}, \gamma_1) = (0.4, 0.2, 28.0)$, it can be seen that the maximum yield occurs in the unstable region. The optimum operation of the reactor requires therefore a tight control around the unstable point.

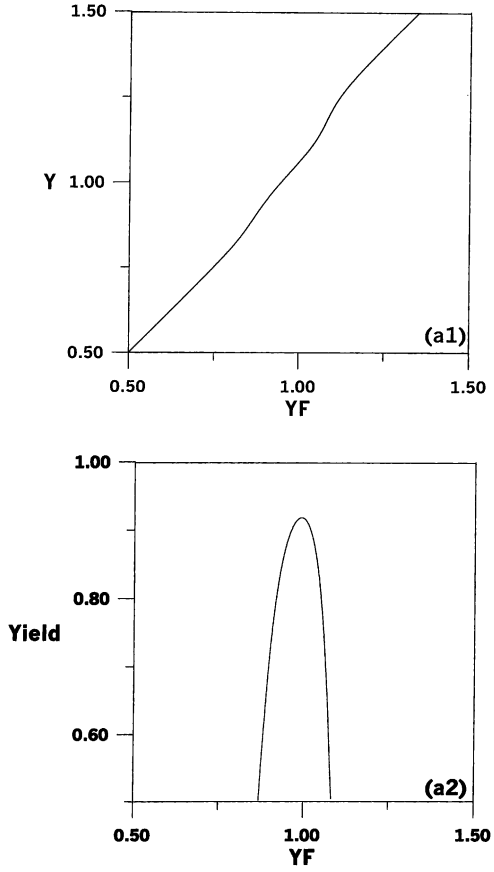

Fig. 4. Continuity diagrams of temperature and yield for region (a) of Fig. 3.

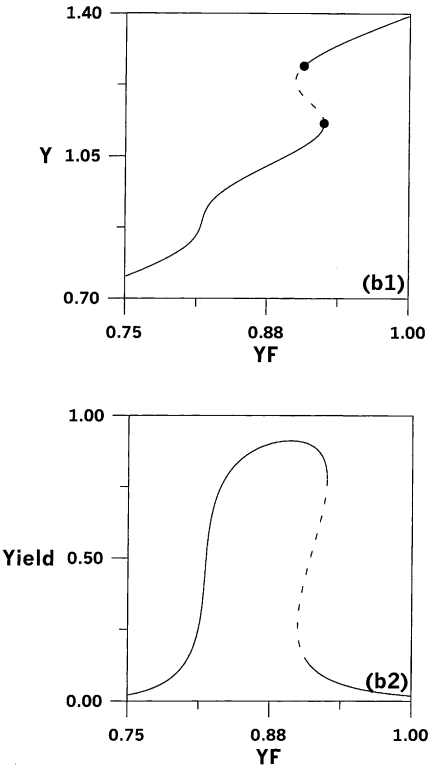

Fig. 5. Continuity diagrams of temperature and yield for region (b) of Fig. 3, solid — stable branch; dash — unstable; circle — static limit point.

3.2. Double limit singularity

The existence of four static limit points in the model is an indication of potential richness, since the relative location of the limit points can change in the bifurcation diagrams. A typical example of this behavior is provided by the double limit singularity (Fig. 2(d) and (e)) where the number of static limit points does not change but their relative positions do. This singularity is defined by the following relations

$$F(Y_1) = F(Y_2) = 0 \tag{11}$$

and

$$F_Y(Y_1) = F_Y(Y_2) = 0 \tag{12}$$

with

$$Y_1 \neq Y_2 \tag{13}$$

These relations require that two distinct points Y_1 and Y_2 should satisfy steady state and also limit point conditions. Fig. 9 shows the boundaries of the double limit singularity in the parameter space $(X_{A_f}, \bar{\beta})$. The region of four static limit points (region (c) of Fig. 3) can be in fact divided in two different subregions. Fig. 10(c_1) and (c_2) show the static behavior for regions c_1 and c_2, respectively. It can be seen that the relative location of the limit points (SLP_2) and

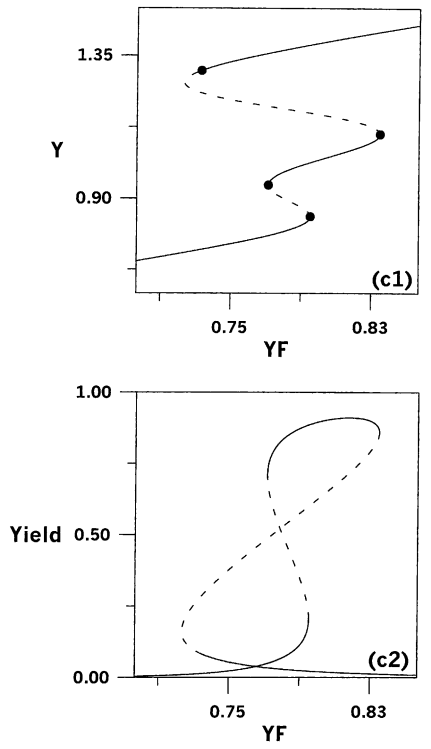

Fig. 6. Continuity diagrams of temperature and yield for region (c) of Fig. 3, solid — stable branch; dash — unstable; circle — static limit point.

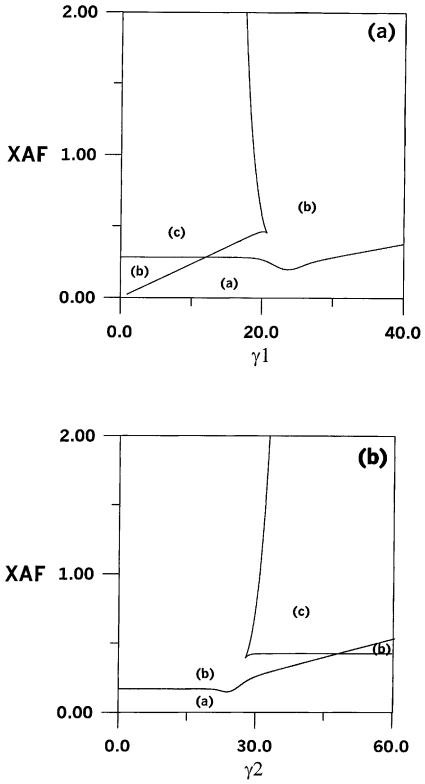

Fig. 7. Branch sets for the hysteresis singularity in the parameter space (X_{A_f}, γ_1) and (X_{A_f}, γ_2).

(SLP_4) has changed in the two diagrams. This has the practical effect of narrowing the range of the middle stable region (between SLP_2 and SLP_3) in region c_2. The maximum yield is therefore likely to occur at an unstable branch in this region. The double limit variety can also be seen as horizontal lines in the parameter spaces (X_{A_f}, Le_A) and (X_{A_f}, Le_B) (Fig. 11(a) and (b)).

3.3. Isola and mushroom

The third possible qualitative change that can occur in the steady-state locus is the appearance of an isola (Fig. 2(b)) and the growth of an isola into a mushroom (Fig. 2(c)).

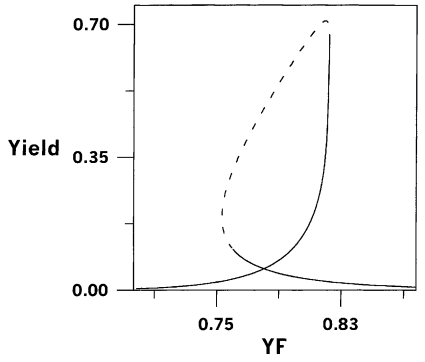

Fig. 8. Continuity diagram for region (b) of Fig. 7(a) showing the maximum yield occurring in the unstable region.

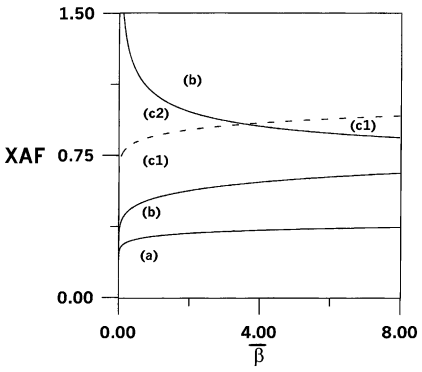

Fig. 9. Branch sets for the double limit singularity in the parameter space $(X_{A_f}, \bar{\beta})$, solid — boundary for the hysteresis singularity; dash — boundaries for the double limit singularity.

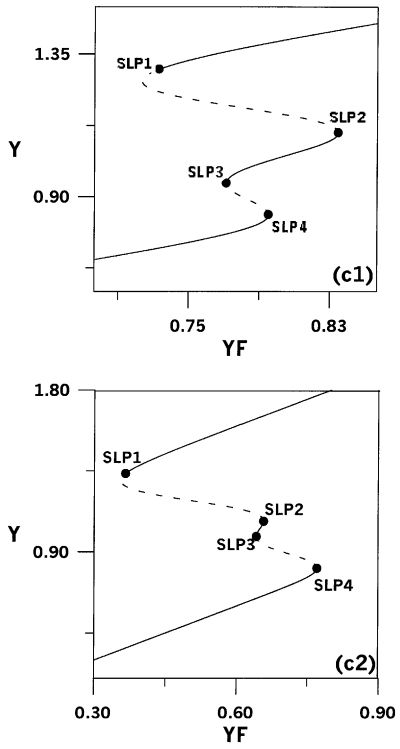

Fig. 10. Continuity diagrams in regions c_1 and c_2 of Fig. 9. The position of SLP_2 and SLP_4 has changed, solid — stable branch; dash — unstable; circle — static limit point.

The requirements for these two changes in the steady-state behavior are that

$$F = F_Y = F_{Y_f} = 0 \tag{14}$$

with the additional requirements that

$$F_{YY_f} \neq 0, \qquad F_{YY} \neq 0, \qquad F_{Y_f Y_f} \neq 0 \tag{15}$$

Taking the derivative of Eq. (6) with respect to (Y_f) yields

$$-F_{Y_f} = \alpha_1\alpha_2\bar{\beta}\exp\left(-\frac{\gamma_1+\gamma_2}{Y}\right) + \alpha_1\bar{\beta}^2\exp\left(-\frac{\gamma_1}{Y}\right) + \alpha_2\bar{\beta}^2\exp\left(-\frac{\gamma_2}{Y}\right) + \bar{\beta}^3 \tag{16}$$

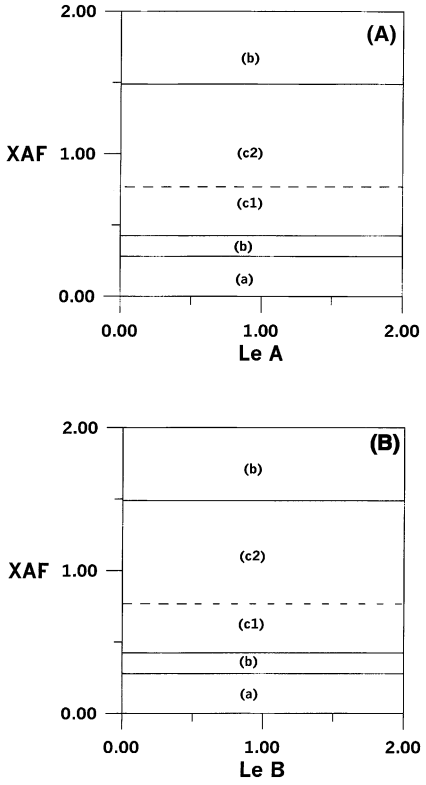

Fig. 11. Branch sets for the double limit singularity in the parameter space (X_{A_f}, Le_A) and (X_{A_f}, Le_B), solid — boundary for the hysteresis singularity; dash — boundaries for the double limit singularity.

Since all the terms involved in this equations are positive, the requirement that F_{Y_f} vanishes is satisfied only for the physically unrealistic case of $\bar{\beta} = 0$. The model, therefore, cannot exhibit an isola or mushroom singularity. The same result holds for any bifurcation parameter other than Y_f.

3.4. Pitchfork and higher order singularities

In order for the single scalar function to undergo a pitchfork bifurcation (Fig. 2(f)) it is sufficient to have

$$F = F_Y = F_{Y_f} = F_{YY} = 0 \tag{17}$$

and

$$F_{YY_f} \neq 0, \qquad F_{YYY} \neq 0 \tag{18}$$

Under these conditions the function F is equivalent to a pitchfork normal form. Since the condition of the existence of a pitchfork includes the condition $(F_{Y_f} = 0)$ as in the case of isola and mushroom, the model, therefore, cannot exhibit codimension two singularity or a higher one.

The analysis of the static bifurcation has revealed that the double limit variety is the highest singularity the model can predict. In the next section we carry out an investigation of the dynamic bifurcation of the model.

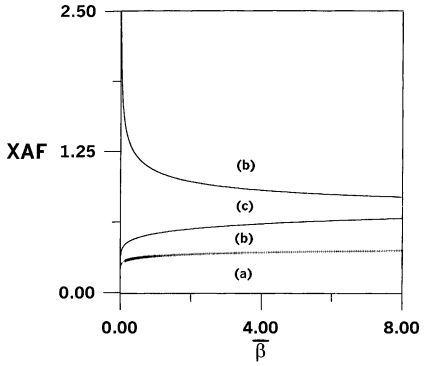

Fig. 12. Complete static and dynamic branch set in the parameter space $(X_{A_f}, \bar{\beta})$, solid — hysteresis branch set; bold — Hopf bifurcation curve.

4. Dynamic bifurcation

The existence of periodic solutions, i.e. Hopf points in the model is associated with a change in the equilibrium of singular points when a single pair of eigenvalues of the linearized system crosses the imaginary axis. The three-dimensional system has a Hopf bifurcation point

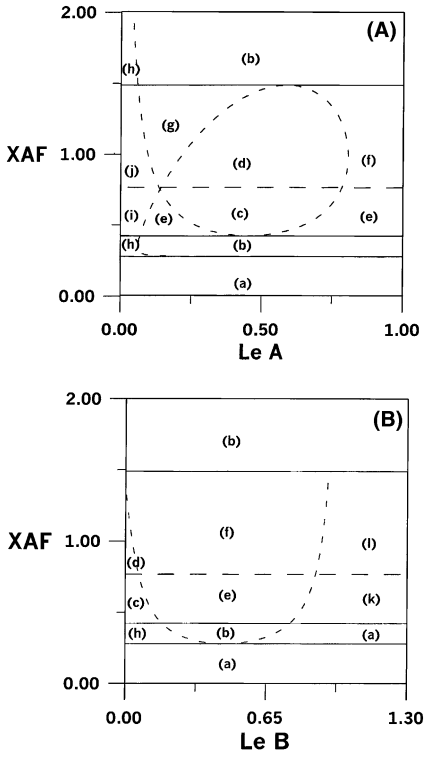

Fig. 13. Complete static and dynamic branch set in the parameter space (X_{A_f}, Le_A) and (X_{A_f}, Le_B), solid-hysteresis branch set; dash-Hopf bifurcation curve; semi dash – double limit singularity.

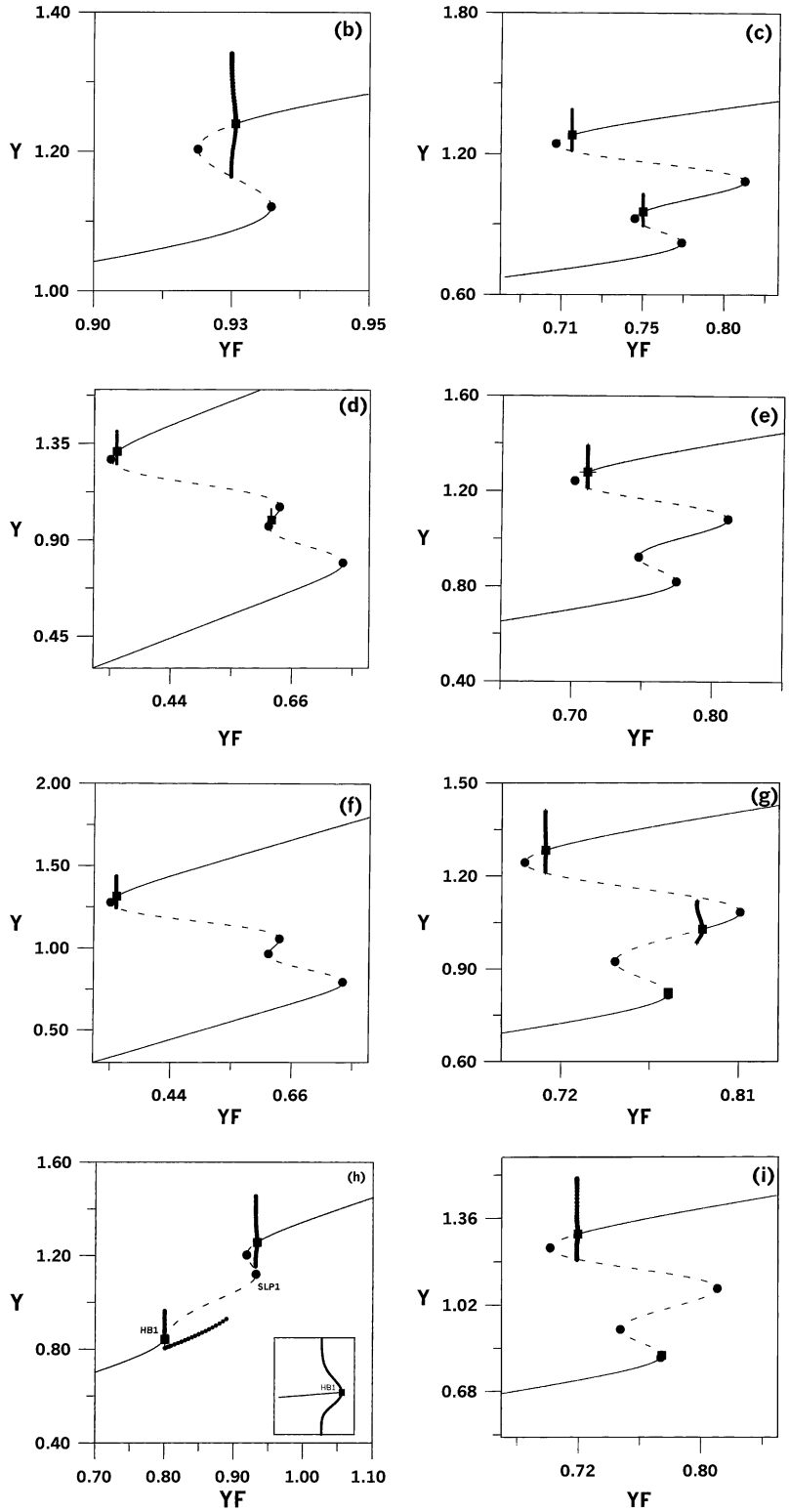

Fig. 14. Continuity diagrams for the nine regions (b)–(j) of Fig. 13(a), solid — stable branch; dash — unstable; circle — static limit point; square — Hopf point; bold line — periodic branch.

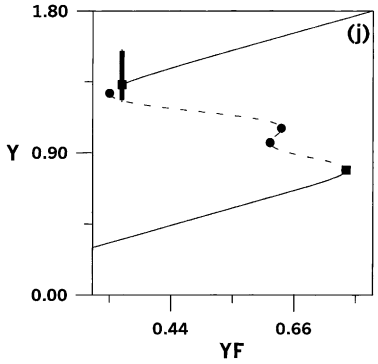

Fig. 14. (*Continued*).

when the Jacobean matrix has pure imaginary eigenvalues. The Jacobean matrix for this model is

$$J = \begin{bmatrix} f_{1X_A} & f_{1X_B} & f_{1Y} \\ f_{2X_A} & f_{2X_B} & f_{2Y} \\ f_{3X_A} & f_{3X_B} & f_{3Y} \end{bmatrix} \tag{19}$$

where f_1, f_2 and f_3 denote the right-hand sides of the mass balances (Eqs. (1)–(3)). The eigenvalue λ of the Jacobean matrix are the solutions of the characteristic matrix equation,

$$-\lambda^3 + S_1\lambda^2 - S_2\lambda + S_3 = 0 \tag{20}$$

where S_1, S_2 and S_3 are the three invariants of J,

$$S_1 = j_{11} + j_{22} + j_{33} \tag{21}$$

$$S_2 = \det\begin{pmatrix} j_{11} & j_{12} \\ j_{21} & j_{22} \end{pmatrix} + \det\begin{pmatrix} j_{22} & j_{23} \\ j_{32} & j_{33} \end{pmatrix} + \det\begin{pmatrix} j_{11} & j_{13} \\ j_{31} & j_{33} \end{pmatrix} \tag{22}$$

$$S_3 = \det(J) \tag{23}$$

The j_{11}, j_{12}, ... are the elements of J. The conditions of Hopf bifurcation in terms of the coefficients S_1, S_2 and S_3 can be derived by setting $\lambda = iw$ into Eq. (20) to yield,

$$F_1 := S_1S_2 - S_3 = 0 \tag{24}$$

$$S_2 > 0 \tag{25}$$

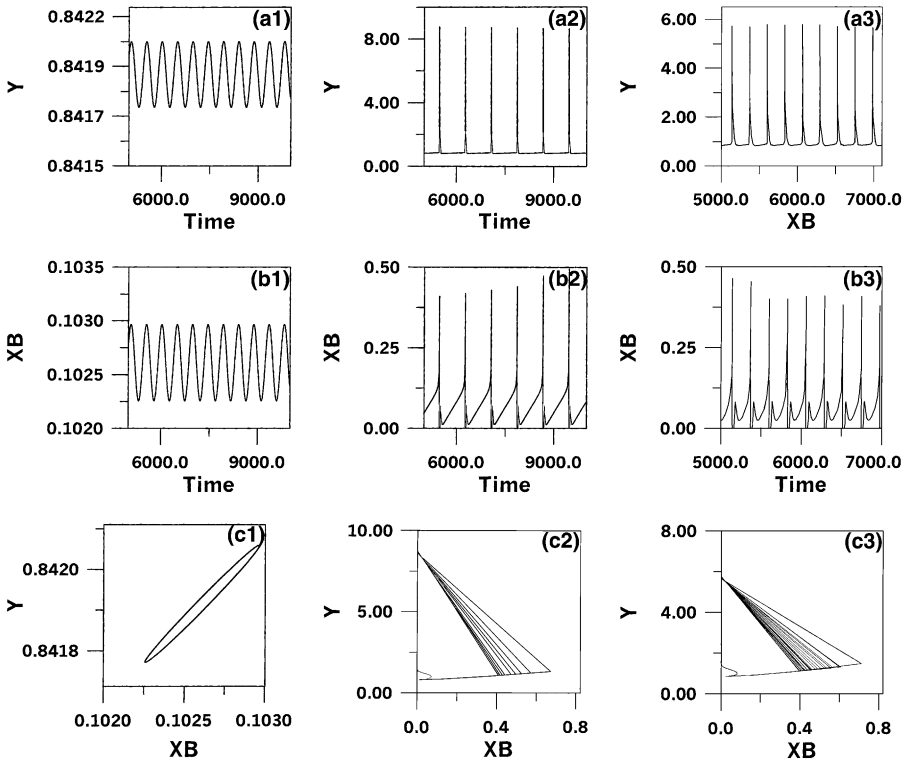

Fig. 15. Time traces showing the burst in temperature in the periodic branch of region (h): (a_1–c_1) $Y_f = 0.800857$; (a_2–c_2) $Y_f = 0.8009$; (a_3–c_3) $Y_f = 0.830$.

4.1. Codimension 1 singularity

The simplest interactions between a Hopf point and a static limit point occurs when the imaginary part of the complex conjugate eigenvalue pair goes to zero. This degeneracy, called the F_1 degeneracy [1], is defined by solving the steady-state equation ($F = 0$) (Eq. (6)), the condition $S_2 = 0$ and the static limit point conditions $S_3 = 0$. Fig. 12 shows the complete static and dynamic bifurcation diagrams in the parameter space $(X_{A_f}, \bar{\beta})$. When crossing the boundaries for the F_1 curve the number of Hopf points in the continuity diagrams increases/decreases by one. It can be seen that in the parameter space $(X_{A_f}, \bar{\beta})$ (Fig. 12), the Hopf boundary is almost identical to the lower boundary separating regions (a) and (b). Therefore, the model admits a Hopf point in all the regions of multiplicity, i.e. regions above (a). The complete static and dynamic branching can be better seen in the parameter space (X_{A_f}, Le_A) and (X_{A_f}, Le_B) (Fig. 13). It can be seen that the hysteresis boundaries are insensitive to changes in the Lewis numbers. They do not affect the static behavior, since they do not appear in the static equation (Eq. (6)). The F_1 degeneracy curve (indicated by a dash line) forms a loop tangent to two static branches and also crosses the double limit variety. This adds interesting features to the system behavior as a total of 10 qualitatively different regions can be delineated.

Region (a) is characterized as in Fig. 4(a_1) with the absence of static or Hopf point, i.e. unique stable solutions. When crossing region (b) two static limit point (SLP) and a Hopf point (HB) are born, since both the hysteresis and the F_1 lines are crossed. The continuity diagram for this region, (Fig. 14(b)), shows three steady-state branches and also stable periodic branches in the vicinity of the Hopf point. The periodic branches emanating from the HB terminate homoclinically as they collide with the static branches. When moving to region (c) two extra limit points and an extra Hopf point are born, since both the hysteresis and the F_1 curve are again crossed. This region is characterized, respectively, by the occurrence of SLP, SLP, HB, SLP, SLP, HB points.

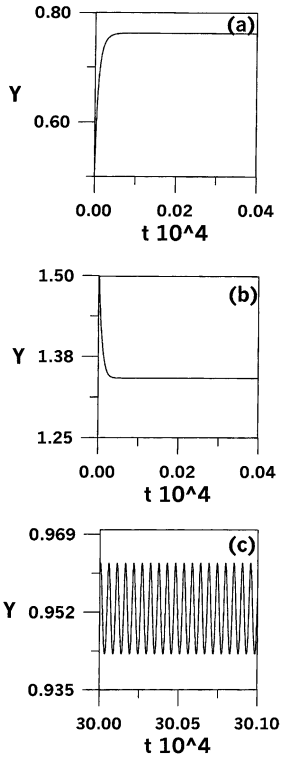

Fig. 16. Time traces showing multistability, (a) high temperature attractor obtained with initial conditions $(X_A, X_B, Y) = (0.5, 0, 0.5)$; (b) low temperature attractor obtained with initial conditions $(X_A, X_B, Y) = (0.01, 0., 1.5)$; (c) period oscillations obtained with initial conditions $(X_A, X_B, Y) = (0.10049, 0.4984, 0.9525)$.

Fig. 14(c) shows the continuity diagram in this region. Again the two Hopf points introduce stable periodic behavior in two different regions of the parameter space. When crossing the line of double limit variety (region (d)), the number of static and Hopf points does not change although their relative positioning do, as shown in Fig. 14(d). Moving to region (e), one Hopf point disappears as one branch of the F_1 curve is crossed and the system is characterized,

Table 2
Summary of the stability characteristics for the different regions of the branch sets[a]

Region	Figures	Static and dynamic bifurcation points
a	3, 7(a) and (b), 13(a) and (b)	Uniqueness
b	3, 7(a) and (b), 13(a) and (b), 14(b)	SLP, SLP, HB
c	13(a) and (b), 14(c)	SLP, SLP, HB, SLP, SLP, HB
$d^{(*)}$	13(a) and (b), 14(d)	SLP, SLP, HB, SLP, SLP, HB
e	13(a) and (b), 14(e)	SLP, SLP, SLP, SLP, HB
$f^{(*)}$	13(a) and (b), 14(f)	SLP, SLP, SLP, SLP, HB
g	13(a), 14(g)	HB, SLP, SLP, HB, SLP, SLP, HB
h	13(a) and (b), 14(h)	HB, SLP, SLP, HB
i	13(a), 14(i)	HB, SLP, SLP, SLP, SLP, HB
$j^{(*)}$	13(a), 14(j)	HB, SLP, SLP, SLP, SLP, HB
k	13(b)	SLP, SLP, SLP, SLP
$l^{(*)}$	13(b)	SLP, SLP, SLP, SLP

[a] The region indicated by (∗) and the region directly before it are located on opposite sides of the double limit variety. Therefore, the relative location of SLP changes in the two regions.

respectively, by the occurrence of four limit points and a Hopf point (SLP, SLP, SLP, SLP, HB). The continuity diagram is shown in Fig. 14(e). When crossing the double limit variety (region (f)) the same number of limit points and Hopf points is found, although the relative positioning of limit points change, as shown in Fig. 14(f).

When crossing region (g) three branches of the F_1 degeneracy curve are crossed and therefore a third HB point appears. Region (g) is characterized with the presence in this order of HB, SLP, SLP, HB, SLP, SLP, HB. The continuity diagram is shown in Fig. 14(g). The third Hopf can be seen to lie close to the static limit point. Three regions of periodic behavior can be found in the model.

When moving from region (g) to region (h) one HB point disappears as well as two static limit points. Region (h) is characterized by the presence in this order of HB, SLP, SLP, HB (Fig. 14(h)). This region has interesting features, since it is the only region in the diagram where sustained oscillations do not coexist with any static branch. For any values of Y_f between the smallest Hopf point (HB_1) ($Y_f = 0.800857$) and the first limit point (SLP_1) ($Y_f = 0.932258$), the system will settle on sustained oscillations for any choice of initial conditions. Moreover the stable periodic branch emanating from the Hopf point HB_1 loses its stability through Torus bifurcation and the resulting oscillations present a quite dangerous situation for the reactor since a sudden 'burst' in temperature is observed all along the periodic region. This situation is explained in Fig. 15 showing time traces and phase plane diagrams for three values of the feed temperature Y_f. Very close to the Hopf point, i.e. $Y_f = 0.800857$, the system, as expected, exhibits a stable limit cycle with small oscillations (Fig. 15(a_1)–(c_1)). However, when the feed temperature Y_f moves even slightly higher ($Y_f = 0.8009$) a dangerous burst in the temperature occurs. The temperature jumps to very high values (more than 8.5), exceeding more than 10 times the mean value of $Y = 0.8$ for the limit cycle. This sudden burst is also accompanied by a lost of stability as it can be seen in the time trace of intermediate component (B) (Fig. 15(b_2)) and in the phase plane (Fig. 15(c_2)). These diagrams suggest a quasi-periodic behavior. The maximum Lyapunov exponent, computed by the algorithm of Wolf et al. [17], is zero further confirming the quasi-periodic nature of the attractor. As the feed temperature moves to higher values, ($Y_f = 0.830$) the oscillations become more erratic and the same dangerous situation prevails (Fig. 15(a_3)–(c_3)). The maximum Lyapunov exponent of the system is 0.02145 confirming the chaotic nature of the oscillations. It should be also noted that the system, for this region (h), also admits a smaller region of periodic behavior around the second Hopf point (HB_2) ($Y_f = 0.933797$). However, these oscillations coexist with the static branch.

Moving to regions (i) and (j), two static limit points are born as well as a Hopf point. Regions (i) and (j) are characterized by the presence in this order of HB, SLP, SLP, SLP, SLP, HB. The relative location of limit points changes in regions (i) and (j) (Fig. 14(i) and (j)) since they are located on the different sides of the double limit variety.

Some of these 10 regions can be found in Fig. 13(b) showing the complete branching phenomena in the parameter space (X_{A_f}, Le_B). However, two new regions are added by this diagram. Region (k) is characterized by the occurrence of four static limit points but with no Hopf points. Region (l) is similar to region (k) expect for the relative location of the static limit points.

In all of these regions (expect regions (a, h, l, k)) the location of the periodic branch between static branches introduces in the system the phenomenon of multistability where self sustained oscillations coexist with the high and low conversion static branch. Fig. 16(a)–(c) show time traces for (X_{A_f}, Le_A, Y_f) = (0.6, 0.5, 0.75213) and for three sets of initial conditions. The periodic behavior in this region is not orbitally stable since different initial conditions can break it and push it out of its domain of attraction, resulting in the annihilation of the oscillations. Tables 2 and 3 summarize the stability characteristics of the 12 regions found in the parameter space (X_{A_f}, Le_A) and (X_{A_f}, Le_B).

A final note should be made about the impact of oscillatory behavior on the yield of the intermediate product.

Table 3
Summary of the stability characteristics for the different regions of the branch sets

Region	Coexistence of oscillations with low temperature branch	Coexistence of oscillations with high temperature branch	Coexistence of oscillations with middle temperature branch	Existence of oscillations alone
a	N	N	N	N
b	Y	N	N	N
c	Y	Y	Y	N
d	Y	Y	Y	N
e	Y	N	N	N
f	Y	N	N	N
g	Y	Y	N	N
h	Y	N	N	Y
i	Y	N	N	N
j	Y	N	N	N
k	N	N	N	N
l	N	N	N	N

Different simulations were carried out in regions of periodic behavior. They have shown that the average yield deteriorates in these regions and thus oscillatory behavior is to be eliminated either by choosing appropriate startup conditions or by a tight control.

5. Conclusions

A general and useful picture of static and dynamic branching phenomena in a gas–solid bubbling fluidized-bed catalytic reactor has been constructed using the singularity theory and continuation techniques. Both the static and dynamic equations were expressed as single algebraic equations. It was shown that the highest static singularity the system can exhibit is the double limit variety. Three different static regions were found in the system: a region of uniqueness, region of three solutions and regions of maximum five solutions. The analysis of dynamic bifurcation has shown that the system can predict codimension one singularities for a wide range of parameters. The complete static and dynamic bifurcation analysis was useful in delineating a total of 12 dynamically different regions. Periodic behavior can be found in 10 regions. In 9 of the 10 regions the sustained oscillations are not orbitally stable since they coexist with low and high temperature static branches. However, in one region sustained aperiodic oscillations can be found that do not coexist with any static branches as they are the sole attractors to the system. However, these oscillations present a dangerous situation for the system as a sudden burst in the temperature is observed, requiring therefore a tight control of the reactor. The effect of the branching phenomena on the yield of the intermediate product has shown that the maximum yield can occur for some regions in unstable branches and that oscillatory behavior deteriorates the yield and should be controlled.

Appendix A. Derivation of the model of the fluidized-bed catalytic reactor

The following assumptions are used in the derivation of the unsteady-state mass and energy balance for the reactor model.

- The gas in the bubble phase is assumed to be in plug flow.
- The dense phase gas is perfectly mixed. This assumption is justified for strongly adsorbed gases.
- The extent of the reaction in the bubble-cloud phase is negligible. This assumption is justified for small particles size ($d_p \leq 150\,\mu m$) and high flow rates giving rise to fast rising bubbles and negligible cloud phase.
- Negligible mass and heat transfer resistances between the solid particles and the dense phase gas.
- An average value of bubble size and hence an average value of the exchange parameters between the dense and bubble phase are used.
- Negligible heat of adsorption.
- Both reactions are of first order.

Unsteady state mass balance for the dense phase:

$$\phi_i A_I H \frac{dC_i}{dt} = G_I(C_{if} - C_i) + Q_{Ei} A_C \int_0^H (\bar{C}_i - C_i)\, dh - \rho_s(1-\epsilon) A_I H R_i \quad (A.1)$$

Unsteady state heat balance for the dense phase:

$$\phi_H A_I H \frac{dT}{dt} = G_I \rho_f C_{pf}(\bar{T}_f - T) + \rho_f C_{pf} Q_H A_C \times \int_0^H (\bar{T} - T)\, dh + A_I H(1-\epsilon)\rho_s \times \sum_{i=1}^{2} r_i(-\Delta H_i) \quad (A.2)$$

Mass and heat balances in the bubble phase:

Both the mass balances and heat balances are assumed at at pseudo-state because of negligible mass and heat capacities, and are given by

$$G_C \frac{d\bar{C}_i}{dh} = -Q_{Ei} A_C(\bar{C}_i - C_i) \quad (A.3)$$

$$G_C \frac{d\bar{T}}{dh} = -Q_{EH} A_C(\bar{T} - T) \quad (A.4)$$

with the boundary conditions,

$$\text{At } h = 0,\ C_i = C_{if} \quad \text{and} \quad \bar{T} = \bar{T}_f \quad (A.5)$$

Eqs. (A.3)–(A.5) are solved analytically. The resulting solutions are used to evaluate the integral in Eqs. (A.1) and (A.2). Assuming that $Q_{EA} = Q_{EB} = Q_{EC} = Q_H$ and casting the equations in dimensionless form gives the model equations as described in the text.

The yield of the reactor is given by

$$y = \frac{G_I X_B + G_C \bar{X}_{BH}}{(G_I + G_C) X_{A_f}} \quad (A.6)$$

where

$$\bar{X}_{BH} = X_B + (X_{B_f} - X_B)e^{-a} \quad (A.7)$$

and

$$a = \frac{Q_E H A_C}{G_C} \quad (A.8)$$

$\bar{\beta}$ is the reciprocal of the effective residence time of the bed and is given by

$$\bar{\beta} = \frac{G_I + G_C(1 - e^{-a})}{A_I H} \quad (A.9)$$

Calculation of the two-phase model parameters [18–21]:

$$G_B = A(U - \phi U_{mf}) \quad (A.10)$$

$$G_C = G_B\left(1.0 + \frac{\epsilon}{\alpha - 1.0}\right) \quad (A.11)$$

$$G_I = AU - G_C \quad (A.12)$$

$$A_C = \frac{\epsilon G_B}{(\alpha - 1.0)U_{mf}} \quad (A.13)$$

$$A_I = A - A_C \quad (A.14)$$

References

[1] M. Golubitsky, D. Schaeffer, Singularities and Groups in Bifurcation Theory, Vol. 1, Springer, New York, 1985.
[2] V. Balakotaiah, D. Luss, Chem. Eng. Sci. 37 (1982) 1611.
[3] H. D'anna, P.G. Lingola, S.K. Scott, Proc. R. Soc. London, Ser. A 403 (1986) 341.
[4] K. Alhumaizi, R. Aris, Surveying Dynamical System: a Study of the Gray–Scott Reaction in a Two-phase Reactor, Longman, UK, 1995.
[5] S. Subramanian, V. Balakotaiah, Chem. Eng. Sci. 52 (1997) 961.
[6] W.M. Edwards, H.N. Kim, Chem. Eng. Sci. 37 (1988) 1611.
[7] S.S.E.H. Elnashaie, M.M.K. Fouad, S.S. Elshishini, Math. Comput. Model. 13 (1990) 11.
[8] K.M. Wagialla, A.M. Helal, S.S.E.H. Elnashaie, Math. Comput. Model. 15 (1991) 27.
[9] S.S.E.H. Elnashaie, K.M. Wagialla, A.M. Helal, Math. Comput. Model. 15 (1991) 43.
[10] R. Aris, The Mathematical Theory of Diffusion and Reaction in Permeable Catalyst, Vol. 2, Oxford University Press, Oxford, 1975, p. 162.
[11] W.H. Ray, S.P. Hastings, Chem. Eng. Sci. 35 (1980) 589.
[12] E.W. Arnold, S. Sundaresan, AIChE J. 35 (1989) 746.
[13] A. Il'n, D. Luss, AIChE J. 38 (1992) 1609.
[14] K.Y. Choi, W.H. Ray, Chem. Eng. Sci. 41 (1985) 2261.
[15] S.S.E.H. Elnashaie, S.S. Elshishini, Chem. Eng. Sci. 48 (1993) 567.
[16] E.J. Doedel, J.P. Kernevez, AUTO: Software for Continuation and Bifurcation Problems in Ordinary Differential Equations, California Institute of Technology, Pasadena, 1986.
[17] A. Wolf, J.B. Swift, H.L. Swinney, J.A. Vastano, Phys. D 16 (1985) 285.
[18] B.A. Partridge, P.N. Rowe, Trans. Inst. Chem. Engrs. 44 (1966) 335.
[19] C. Chavarie, J.R. Grace, Ind. Eng. Chem. Fund. 14 (1975) 87.
[20] J.F. Davidson, D. Harrisson, R.D. La Nauze, R.C. Darton, in: L. Lapidus, N.R. Amundson (Eds.), Chemical Reactor Theory: A Review, Prentice-Hall, Englewood Cliffs, NJ, 1977 (Chapter 10).
[21] D.B. Bukur, in: L.K. Daraiswamy, B.D. Kulkarni (Eds.), Transport Processes in Fludized Bed Reactors, Wiley Eastern Limited, New Delhi, 1987 (Chapter 5).